IEEE Access
Multidisciplinary ⋮ Rapid Review ⋮ Open Access Journal

Received 19 December 2024, accepted 6 January 2025, date of publication 10 January 2025, date of current version 17 January 2025.

Digital Object Identifier 10.1109/ACCESS.2025.3528081

RESEARCH ARTICLE

Parametric Study and Experimental Validation of Acoustic Leaky Wave Antenna in Spatial Localization

ALEJANDRO FERNÁNDEZ-GARRIDO[1], MARÍA CAMPO-VALERA[2], ELENA ABDO-SÁNCHEZ[2], (Member, IEEE), RUBÉN PICÓ[3], ANTONIO-JAVIER GARCIA-SANCHEZ[1], AND RAFAEL ASOREY-CACHEDA[1], (Member, IEEE)

[1]Department of Information and Communications Technologies, Universidad Politécnica de Cartagena, 30202 Cartagena, Spain
[2]Telecommunication Research Institute (TELMA), Universidad de Málaga, 29071 Málaga, Spain
[3]Institut d'Investigació per a la Gestió Integrada de les Zones Costaneres (IGIC), Universitat Politècnica de València (UPV), 46730 Gandia, Spain

Corresponding author: Alejandro Fernández-Garrido (alejandro.fernandez3@upct.es)

This work was supported in part by the ThinkInAzul and AgroAlNext Programs funded by Ministerio de Ciencia, Innovación y Universidades (MICIU) with funding from European Union (EU) NextGenerationEU/Plan de Recuperación, Transformación y Resiliencia (PRTR)-C17.I1; in part by the Fundación Séneca with funding from Comunidad Autónoma Región de Murcia (CARM); in part by the MICIU/Agencia Estatal de Investigación (AEI)/10.13039/501100011033 under Grant PID2023-148214OB-C21, Grant TED2021-129336B-I00, Grant PID2022-141193OB-I00, and Grant PID2022-138321NB-C22; in part by the European Union NextGenerationEU/PRTR and Fondo Europeo de Desarrollo Regional (FEDER)/EU; and in part by the Fundación Séneca under Grant 22236/PDC/23.

ABSTRACT Acoustic signals, which have been utilized for decades in the spatial localization of objects, have found applications in fields as diverse as sonar for underwater navigation, communication, and object detection. Traditional methods often rely on arrays of transducers, which necessitate the use of expensive hardware and processing algorithms. An emerging alternative is the Acoustic Leaky Wave Antenna (ALWA), which is inspired by electromagnetic leaky wave antennas. ALWA technology employs a single transducer to emit directional beams that scan angular space by frequency manipulation. Conventional arrays offer cost-effectiveness and simplicity of design, but ALWAs have the advantage of operating on the principle of energy leakage, which is achieved by various mechanisms, such as uniform apertures or slits periodic along the waveguide. This technology, applicable to underwater and airborne communications, offers compact and energy-efficient solutions, which facilitate the development of the ''Underwater Internet of Things'' and autonomous communication systems for underwater vehicles. This work presents a parametric study of this type of antennas with axisymmetric geometry by means of a numerical solution based on the Finite Element Method. Together with analytical studies, the physical phenomenology underlying this technology will be described, including directivity, transmission and reflection parameters, beam scanning and dispersion curve. Finally, the design is validated through experiments.

INDEX TERMS Acoustic leaky-wave antennas, beam scanning, propagation, directivity, finite element method, underwater acoustic.

I. INTRODUCTION

For decades, acoustic signals have been utilized for the purpose of locating objects in space. One illustrative example is SONAR, a localization and tracking technique that employs underwater sound propagation for navigation, communication, the detection of submerged objects, and the measurement of distance [1]. Additionally, other airborne sound localization applications have been developed, including security systems and sound radiation mapping, which aim to reduce noise emissions from vehicles, machinery, and appliances, among others. In all these cases, arrays of microphones or transducers in different geometric configurations are employed [2], [3], [4]. The simultaneous processing of

The associate editor coordinating the review of this manuscript and approving it for publication was Yougan Chen.

the channels necessitates the use of costly dedicated hardware and computationally demanding processing algorithms, which in turn results in a significant increase in power consumption.

An alternative technique that is demonstrably more advantageous than the use of arrays is the use of Acoustic Leaky Wave Antennas (ALWAs). The ALWA concept is inspired by Leaky Wave Antennas (LWAs) of the electromagnetic domain, as described in [5]. Its transfer to the acoustic domain is rather recent, having been first introduced in 2013 by Naify et al. [6]. The interest in ALWAs with respect to other types of acoustic technologies is due to their use of a single transducer that emits directional beams that scan the angular space. This is achieved by varying the feeding frequency of the acoustic waveguide, as demonstrated in [7], [8], [9], and [10]. This type of ALWA is suitable for low-cost SONAR applications, as it does not require the use of multiple electronically controlled transducers with phase-scanning techniques typical of conventional designs.

Given the similarities between the electromagnetic and acoustic cases, Bongard et al. [11] introduced the first slotted waveguide acoustic antenna. This antenna includes membrane obstructions in each of the unit cells to form an acoustic metamaterial based on transmission line theory. In [8] experimental evaluations have also demonstrated the advantages of this type of antenna as transmitters over the use of multi-element linear arrays. In other cases, such as in [12] and [13] and taking advantage of the acoustic reciprocity characteristics of ALWA, this technology can also be used as a receiver. By reinforcing a range of frequencies depending on the angle of arrival, it becomes a device capable of providing positional information about a broadband sound source with a single microphone. In [14] an underwater ALWA using an elastic metamaterial as a waveguide was proposed. More recently, in [15] an ALWA antenna with heterogeneous structure is proposed for acoustic source localization applications, which achieves more accurate directivity.

The operational mechanism of an ALWA is based on the radiation phenomenon, which results from the energy leakage through the differents geometries. This leakage can occur via a uniform aperture along a waveguide, or through slots or arrays of shunts positioned at periodic intervals, thereby forming unit cells [16], [17]. Furthermore, the structure can be categorized as heterogeneous [8], [15], [18], [19] or designed based on acoustic metamaterials of the transmission line [11], [20]. The directivity of the radiated energy depends on the frequency of the propagating wave within the guide and the length of the antenna. The orientation of radiation can vary: it may be perpendicular to the waveguide, termed as broadside, tilted in a positive angular direction down to 90°, referred to as endfire, or directed in a negative angular direction down to −90°, known as backfire [21].

This technology, when applied to both underwater and airborne communications, has the potential to significantly advance the development of new solutions that require compact, low-power communication systems.In this context, advanced acoustic antenna technologies have great potential to drive the development of the ‘‘Underwater Internet of Things‘‘ (UIoT) and ‘‘Autonomous Underwater Vehicles‘‘ (AUV), facing significant challenges such as limited data transmission capacity and energy constraints in aquatic environments. These antennas stand out for their efficiency and adaptability to provide effective solutions in contexts where conventional communication systems present limitations, such as acoustic scattering. According to [22], these technologies facilitate the integration of various nodes, from fixed sensors to mobile vehicles, allowing applications in monitoring, deep exploration and generation of early warnings. Thus, these antennas are positioned as a key component in the underwater communication architecture, helping to overcome current barriers and promoting advances in connectivity and operational efficiency.

This work focuses on a parametric study using a numerical solution in air conditions based on the Finite Element Method (FEM), analyzing how geometric changes in the ALWA affect the frequency bandwidth. The goal is to identify which of the proposed configurations effectively broadens this bandwidth.

Building on the initial designs presented in previous research [23], the proposed approach includes an analysis of key parameters, such as the inner radius of the unit cell r_{in}, the thickness of the cell t_{cell}, and the width of the shunt w_{shunt} of the ALWA. The ideal values of these parameters are determined based on bandwidth and angular response. These values can be used to adjust the desired radiation properties of the ALWAS.

Additionally, a comprehensive study of the band structure of the selected final design is conducted to understand how waves interact with the various perturbations present in the waveguide and to observe its operating modes.

Finally, experiments are carried out to contrast the results obtained with the theoretical and numerical studies.

The structure of this paper is organized to provide a comprehensive understanding of the subject matter. Section II outlines the fundamental principles of ALWAs, detailing key aspects such as the propagation constant, scanning angle, and half-power beamwidth (HPBW). Section III then elaborates on the antenna design parameters, using the concentrated element acoustic model for cylindrical waveguides with a single slot and waveguides with periodic slots. In Section IV, the paper describes the methods employed, including both theoretical and numerical approaches. Section V presents the analysis of the results, highlighting the parametric study to identify the most effective design values, such as thickness of the cell, inner cell radius and width of the shunt, based on obtaining a wide frequency bandwidth for this type of antennas. Based on this analysis, the most suitable values are selected to achieve desirable reflection and transmission coefficients, as well as precise radiation patterns, dispersion diagrams, and angular responses. Subsequently, Section VI

details, based on the selected geometrical values, the choice of the material, its construction and the experimental measurements performed. The paper concludes with Section VII, which provides the final remarks, summarizing the key findings and implications of the research.

II. PRINCIPLES OF THE ACOUSTIC LEAKY-WAVE ANTENNA (ALWA)

To facilitate comprehension and tracking of the work, the authors present Table 1, which describes the list of variables used in this paper.

TABLE 1. List of variables.

Variables	Description
A_{inc}	Incident wave amplitude
A_{refl}	Reflected wave amplitude
A_{trans}	Transmitted wave amplitude
c_{ph}	Phase velocity
c_0	Speed of sound in the medium
C_{sh}	Shunt compliance
C_{wg}	Acoustic compliance of the waveguide
f_{Bragg}	Bragg frequency
f_c	Upper cutoff frequency
f_{max}	Maximum simulation frequency
f_{mn}^c	Cut-off frequency of the mode (mn)
f_0	Operating frequency
k_y	The y-component of the wavenumber
k_z	The z-component of the wavenumber
k_0	Free-space wavenumber
l_{wg}	Input/Output waveguide lengths
L	ALWA length
M_{sh}	Shunt mass
M_{wg}	Acoustic mass
p	Pressure
q	Volume velocity
r_{in}	Inner cell radius
r_{out}	Length of unit cell wall
S_a	Cross-sectional area of a waveguide
t_{cell}	Thickness of the unit cell
w_{sh}	Width of the shunt
Y	Shunt admittance
Z	Serie impedance
α	Attenuation constant
$\alpha_{mn}^{'}$	Nth zero of the derivate of the first-species Bessel function
β	Phase constant
γ	Propagation constant
$\Delta\theta$	Half power beamwidth
η_{rad}	Radiation efficiency
θ_r	Radiated angle
λ	Wavelength
ρ_0	Density
ω	Angular frequency

When a periodic modification is introduced into a waveguide structure so that energy can scape, the guided wave leaks power gradually when being propagated [5]. This leakage phenomenon can be exploited strategically in various applications, as discussed in Section I. Figure 1 illustrates the schematic of an ALWA, where the leakage phenomenon is related to a specific directivity within a structure, exemplified by an open waveguide of length L with θ_r representing the radiated angle.

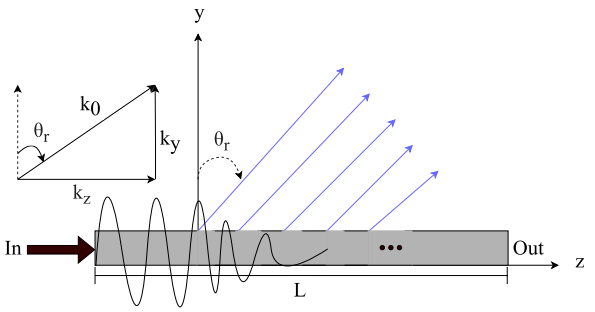

FIGURE 1. Schematic diagram of the structure of an ALWA consisting of a waveguide of length *L* in the z-axis with openings. The blue diagonal lines above the structure represent the sound beams.

The radiated wave of these antennas, in the free region immediately adjacent to the structure, exhibits a general waveform [24], [25] as shown in:

$$P(z, y) = p_0\, e^{-j k_y y} e^{-j k_z z} e^{j\omega t}, \tag{1}$$

where the radiation pattern of the structure is determined by the complex wavenumber k_z [5], [24], [26] in the direction of the waveguide z, and k_y, the propagation constant perpendicular to the waveguide.

The complex wavenumber in the z-direction, k_z, is defined as:

$$k_z = \beta - j\alpha \tag{2}$$

In the configuration of ALWAS, the constants α and β are the attenuation and phase constants, respectively, along the antenna aperture. Specifically, α characterizes leakage rate, which determines the beamwidth, while β determines the radiation angle. In particular, most of the leakage power is radiated near the beginning of the structure and decreases exponentially toward the end, as shown in Figure 1.

Moreover, the propagation constant, k_y, can be approximated as:

$$k_y = \sqrt{k_0^2 - \beta^2} \tag{3}$$

In this analysis, $k_0 = \omega/c$ represents the free-space wavenumber, where c is the sound velocity in the medium, and ω is the angular frequency of the wave. This relationship elucidates two potential scenarios. If the phase velocity of the wave, c_{ph}, is less than the speed of sound in the free field, that is $c_{ph} < c_0$ or $\beta > k_0$, then the constant k_y becomes imaginary. Consequently, the wave in the y-direction becomes evanescent, indicating that it does not propagate through the medium but rather attenuates. Conversely, if the phase velocity exceeds the speed of sound in the free field, $c_{ph} > c_0$ or $\beta < k_0$, k_y is real. This results in leaky-wave propagation at an angle θ_r, where $-\pi < \theta_r < \pi$, as described in [27]. This scenario defines what is known as the "radiation zone" where the wave effectively propagates away from the ALWA.

The propagation constant, β, is related to the scanning angle, θ_r, of the main lobe through the equation (4), according

to the formulation provided in (3):

$$\theta_r = sin^{-1}\left(\frac{\beta}{k_0}\right) \tag{4}$$

According to [5], the beamwidth at half power of the main lobe, $\Delta\theta$, for an ALWA of length L can be approximated by:

$$\Delta\theta \approx \frac{\lambda}{L\,cos\,(\theta_r)} \tag{5}$$

where λ is the wavelength. An important feature of ALWAs is that since the leaky mode phase constant is dispersive with frequency $\beta = \beta(\omega)$, the resulting scanning angle is also frequency dependent $\theta_r = \theta_r(\omega)$. As a result, ALWAs inherently provide frequency scanning of a directional beam [5], [28].

III. PROPOSED DESIGN PARAMETERS

An acoustic waveguide is defined as a structure that guides acoustic waves from one location to another while minimizing energy loss and confining propagation to a specific direction. This confinement is typically achieved through total reflection at the boundaries of the waveguide [29]. This section will focus on the cylindrical waveguides employed in the proposed antenna design, exploring their characteristics and functionality.

A. EQUIVALENT CIRCUIT OF THE WAVEGUIDE WITH SLOT

To design the antenna, a frequency f_0 is selected, targeting a specific frequency for radiation. The frequency f_0 =2700 Hz is chosen because it falls within the audible range and facilitates the construction of the antenna with manageable geometric dimensions.

In the process for the antenna design the concentrated element acoustic model is employed. This approach simplifies the study of an acoustic system in the long wavelength limit i.e. when the wavelength in the medium is significantly larger than the dimensions of the system allowing the assumption that the acoustic pressure is uniform throught the volume of interest. Under these conditions, the acoustic system can be effectively modeled as an ideal concentrated element using electroacoustic analogies [29]. Systems that fulfil this criterion of dimension in relation to wavelength are referred to as concentrated acoustic systems.

The use of electroacoustic analogies involves applying principles from electrical network theory to address acoustic problems by using equivalent parameters. In this approach, the potential difference corresponds to the acoustic pressure p. Similarly, electric current is analogous to the volume velocity q, which flows through the cross-sectional area S_a of a waveguide. A long acoustic tube, acting as a cylindrical waveguide, allows the propagation of plane waves in a fundamental mode without significant transverse variations, similar to the behavior of an electrical transmission line. In this model, the acoustic mass represents the inertia of the air flow (inductors), representing the resistance to changes in velocity caused by acoustic pressure. This is analogous to mechanical

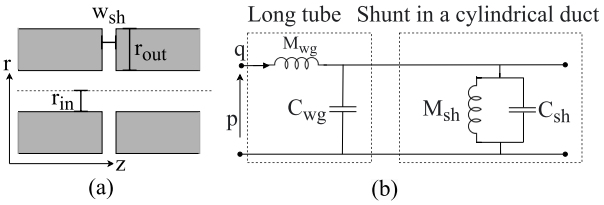

FIGURE 2. Geometry and concentrated acoustic circuit of a slotted waveguide. (a) Tube and shunt, (b) equivalent circuit of the long tube and shunt.

mass. Acoustic compliance (capacitors) describes the ability of the air to compress or expand under acoustic pressure without notable displacement, akin to the behaviour of a mechanical spring that stores and release energy.

In transmission line theory, the circuit configuration illustrated in Fig.2b shows the modelling of a long tube with the shunt with its equivalent circuit [24]. The formulas that govern the mass and acoustic compliance within this section of the waveguide are:

$$M_{wg} = \frac{\rho_0}{S_a}\,dz, \tag{6}$$

$$C_{wg} = \frac{S_a}{\rho_0 c_0^2}\,dz, \tag{7}$$

where ρ_0 is the density of air, dz is the length of the tube and c_0 is the speed of sound in the fluid.

If the waveguide bore takes the form of a slot that symmetrically encircles the central axis in a cylindrical waveguide (known as an axisymmetric slot), the resulting geometry becomes a radial channel. This means that, instead of propagating along the axis of the guide, the waves spread radially, i.e., from the center outward in all directions around the axis. This channel has a length r_{out} and a shunt width w_{sh}, and it connects to the main waveguide, as illustrated in Fig. 2a. Since the axisymmetric slot functions as a radial channel, its input impedance is characterized by using radial transmission line equations, which were originally developed for electromagnetic waves. These equations describe how the propagation constant and characteristic impedance vary with the radial coordinate r, and solutions are typically expressed using Bessel functions [30]. The adaptation of this analysis for acoustic waves can be found in [11].

The formulas governing the mass and acoustic compliance of the shunt are [31]:

$$M_{sh} = \frac{\rho_0}{2\,\pi\,w_{sh}}\,\ln\left(1+\frac{r_{out}}{r_{in}}\right) \tag{8}$$

$$C_{sh} = \frac{1}{4\,\pi^2 f_0^2\,M_{sh}} - C_{wg} \tag{9}$$

where r_{in} corresponds to the inner radius of the waveguide.

B. WAVEGUIDES WITH PERIODICAL SLOTS

By expanding the model in a periodic manner, a set of periodic slots is considered. If these slots are considerably

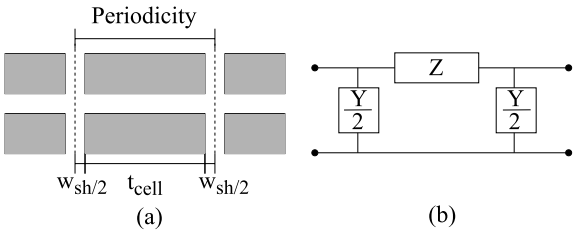

FIGURE 3. Symmetric unit cell model of a waveguide with periodic shunts. (a) Longitudinal view of the cell. The thickness of the cell, t_{cell}, is shown in gray color and the width of the shunt, w_{sh}, is shown in white color, (b) Impedance and admittance circuit.

smaller relative to the wavelength of the guided signal, the waveguide can be divided into unit cells [24] of length t_{cell}. Each of these cells includes a shunt (leakage) with a width of w_{sh}, and the section of the unit cell that connects to the next shunt, as shown in Fig. 3a. Therefore, each cell can be modeled by means of an equivalent circuit, similar to that of the Fig.2b. This approach facilitates the analysis and understanding of the behavior of the waveguide.

The values of the concentrated acoustic elements of the equivalent circuit described in this section are presented in Table 2. These values correspond to the model mentioned in section V-B and have been obtained for an operating frequency of 2700 Hz.

TABLE 2. Values of concentrated acoustic elements.

Variable	Value	Units
M_{wg}	700.28	kg/m^4
C_{wg}	$3.30 \cdot 10^{-12}$	m^3/Pa
M_{sh}	724.64	kg/m^4
C_{sh}	$1.49 \cdot 10^{-12}$	m^3/Pa
S_a	$2.82 \cdot 10^{-5}$	m^2

Using the values provided in Table 2, we can calculate the upper cutoff frequency f_c, which is the highest frequency at which waves can propagate within the ALWA. This calculation is performed using the formula detailed in expression (10) [31]:

$$f_c = \frac{1}{\pi \sqrt{M_{sh}\left(C_{sh} + C_{wg}\right)}} \tag{10}$$

Therefore, the frequency range that can propagate within the antenna extends from $f_0 = 2700$ Hz to $f_c = 5411$ Hz. This defines the preliminary range of interest for this study.

IV. METHODS STUDIED

A. TRANSFER MATRIX METHOD (TMM)

A common approach used to analyze waveguides that exhibit periodic shunts is to segment these structures into unit cells, which allows for accurate and systematic modeling. In this context, each unit cell is represented as a two-port network, while the complete system is modeled as a cascade of multiple two-port connected in series. This technique is called the Transfer Matrix Method (TMM), which establishes clear mathematical relationships between the acoustic input and output variables for each unit cell within the system.

The TMM method is based on the matrix representation of wave propagation through discrete or periodic systems, providing a robust and efficient tool to study the interaction between the shunts and the waveguide. This approach not only allows to accurately characterize the acoustic response of the entire system, but also facilitates the analysis of key properties such as impedance, admittance, transmission and reflection at the unit cell and overall system level.

Each unit cell is strategically located between the midpoints of two consecutive taps, which ensures that the acoustic admittance, represented as Y, is uniform at both the entry point and the exit point of the cell. This arrangement ensures that the symmetry condition, a crucial property fr the correct modeling of the system and for the validity of the analysis using TMM, is met. In Fig. 3b an equivalent circuit describing the configuration of a unit cell and its interaction with adjacent shunts is illustrated. The behavior of this circuit is described by the following equations:

$$Z = j\,\omega\, M_{wg}, \tag{11}$$

$$Y = j\left(\omega\left(C_{sh} + C_{wg}\right) - \frac{1}{\omega\, M_{sh}}\right). \tag{12}$$

In (11) and (12), the impedance Z and admittance Y are imaginary values. This indicates that the phase of the wave propagating through these ducts tends to change, while the amplitude remains constant.

The transmission parameters along the network can be determined using the transmission matrix [$ABCD$]. This matrix characterizes how sound waves behave as they pass through different acoustic elements, such as pipes, walls or other devices, and defines the transfer function of a two-port system. In particular, it establishes the relationship between the sound pressure, p, and the volume velocity, q, at the input and output of the equivalent acoustic circuit of the system under analysis, shown in Fig. 2b. In this way, it facilitates modeling and understanding of how the properties of an acoustic system affect the propagation waves [32]. The transfer matrix is expressed as follows:

$$\begin{bmatrix} p_{in} \\ q_{in} \end{bmatrix} = \begin{bmatrix} A & B \\ C & D \end{bmatrix} \begin{bmatrix} p_{out} \\ q_{out} \end{bmatrix}, \tag{13}$$

where elements A, B, C y D take the following values:

$$A = 1 + \left(\frac{ZY}{2}\right) \tag{14}$$

$$B = Z \tag{15}$$

$$C = Y\left(1 + \frac{Z\,Y}{4}\right) \tag{16}$$

$$D = 1 + \left(\frac{Z\,Y}{2}\right) \tag{17}$$

Once the transfer matrix is obtained, the propagation constant is calculated in terms of the transfer matrix

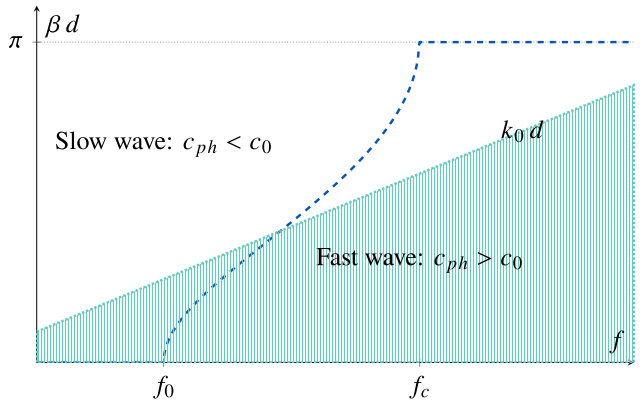

FIGURE 4. Dispersion diagram of a waveguide with periodic slots spaced a distance *d*. Two zones are distinguished, the green zone corresponds to the fast wave and the white zone to the slow wave.

coefficients and the phase factor [32]:

$$\gamma_B = \frac{\operatorname{arcosh}(A)}{t_{cell}}, \tag{18}$$

$$\beta d = \Im\{\gamma_B\}\, t_{cell} \tag{19}$$

To evaluate the performance of the antenna, the dispersion curve is calculated, which indicates the phase shift of the wave in the different periodic sections of the antenna. Each frequency is associated with a different phase velocity ($c_{ph} = \omega/\beta$), as illustrated in Fig. 4. The wavenumber k_0 multiplied by d (denoted as t_{cell} in this work) is included as a reference, which helps to identify the two regions of the dispersion curve: one where the c_{ph} in the duct is greater than speed of sound in air, c_0, and another one where it is smaller.

Fig. 4 illustrates that the bandwidth is bounded by the frequency f_0, where the phase starts to change, and the upper cutoff frequency f_c.

Another key parameter examined is the angular response, which depicts the variation of the antenna scanning angle with frequency. The outcomes of these studies are detailed in Section V.

B. NUMERICAL METHOD

The Finite Element Method (FEM) is a numerical approach to approximate solutions to partial differential equations. This method is extensively employed in engineering to address problems where the analytical solution is either unknown or overly complex to develop. One of its primary advantages is its flexibility in handling complex geometries. The solution domain $\Omega \subset \mathbb{R}^n$ is approximated by a union of smaller disjoint subdomains $\cup\Omega^{(e)}$, known as finite elements, with the problem's nodes located at the vertices of these elements [33]. It is used to obtain more accurate results than those provided by the analytical model, facilitating their comparison.

The preprocessing, processing and postprocessing for the antenna design has been implemented as follows [34]:

1) PREPROCESSING

Given that the proposed antenna design exhibits a symmetry of revolution, it can be treated as an axisymmetric problem. This allows a 3D problem to be simplified into a 2D axisymmetric problem. The response of an acoustic system to a harmonic excitation is simulated.

a: GEOMETRY

The proposed antenna design in this work consists of three main parts. The first two parts are cylindrical waveguide with an input and output length l_{wg}. The third part is a periodic region situated between these cylindrical waveguide. This periodic region comprises several unit cells, denoted as U_{cell}, where $cell = 1, 2, \ldots, 32$. These unit cells have a disc-type geometry and are arranged side by side at a distance w_{sh}. The inner radius of the input and output waveguides is r_{in}, while the outer radius and thickness of the unit cells are r_{out} and t_{cell}, respectively. To achieve a non-reflective boundary, the end of the l_{wg} is filled with an acoustically absorbing material.

The geometry of the proposed antenna, as illustrated in Fig. 5, is axisymmetric. An input acoustic signal with a specified amplitude is introduced at one end of the waveguide and radiates outward through the width (aperture) of the shunt channel w_{sh}. Given that w_{sh} is subwavelength, the antenna can be regarded as a series of point acoustic sources distributed along the z-axis.

b: BOUNDARY CONDITIONS

The boundary conditions used in FEM simulation [35] for the complete antenna structure are described below and illustrated in Fig. 6c:

- Port: This condition is used to model the antenna input and output port which are located at the ends of the input and output waveguides.
- Narrow Region Acoustics (NRA): This condition defines a fluid model for layer-induced losses in constant transverse ducts. Two applications in this work are: (i) circular duct for the waveguide, and (ii) aperture for the shunts between the unit cells.
- Perfectly Matched Boundary (PMB): Applied at the boundary of the simulation domain, since it is a numerical technique that allows to absorb the incident waves on the external contours of the domain and thus avoid unwanted reflections.
- Exterior Field Calculation: This condition allows to calculate the external acoustic pressure field (far field) from the near field transformation, providing the values of the amplitude and the phase of the acoustic field.

For the study of the banding structure, the boundary conditions used in Fig. 6b are:

- Periodic condition: Allows to reduce the size of the model by taking advantage of symmetries and periodicities at the geometrical and physical interfaces. The Floquet periodicity, also called Bloch periodicity, is used.

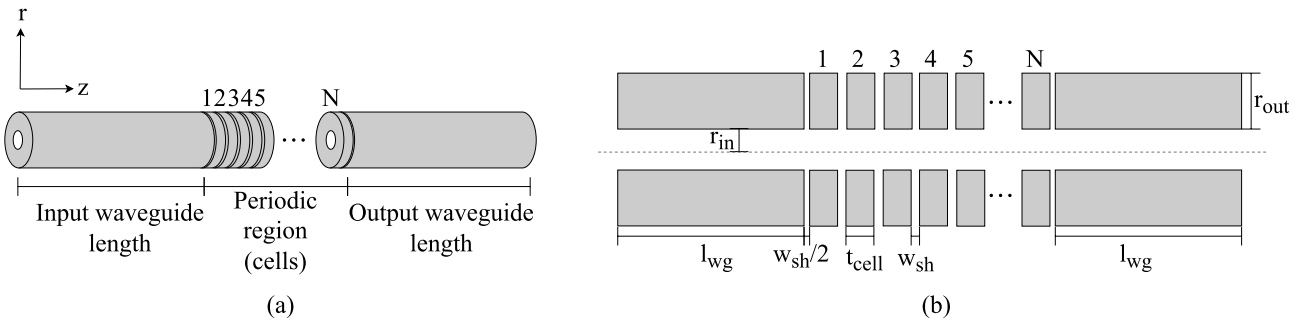

FIGURE 5. Geometry of the proposed design for the ALWA. (a) 3D view, (b) 2D longitudinal plane, where the discontinuous horizontal line represents the symmetry axis of the antenna..

- Impedance: Models the leakage boundary without having to account for the medium through which the antenna radiates.

2) PROCESSING

A mesh with a maximum element size of $\lambda/10$ is used, where λ is the wavelength corresponding to the maximum simulation frequency ($f_{max} = 10\,000$ Hz). Each mesh element has a quadrangular shape to efficiently cover the entire structure without excessive refinement. An example of this is shown in Fig. 6a.

The mesh consists of 2,518,951 domain elements and 33,459 boundary elements with a tetrahedral structure for the complete model.

3) POST-PROCESSING

The acoustic magnitudes represented include the scanning angle according to expression (4), dispersion curve according to expression (19), and transmission and reflection parameters.

- Radiation Pattern: This represents the distribution of the sound intensity emitted by the antenna in various directions. It is obtained using the boundary conditions and variables related to the far field pressure and the sound pressure level. This quantity is used to calculate the beamwidth $\Delta\theta$.
- Scanning Angle: This is determined by identifying the angles at which the pressure level is maximum and plotting the frequencies as a function of these angles.
- Transmission (T) and Reflection (R) Parameters: These parameters provide information about how the incident wave energy is distributed between the reflected and transmitted waves. In the FEM simulation, they are calculated from the S-parameters (scattering parameters):

$$|R| = \frac{A_{refl}}{A_{inc}} = |s_{11}|, \tag{20}$$

$$|T| = \frac{A_{tran}}{A_{inc}} = |s_{21}|, \tag{21}$$

where A_{refl}, A_{inc} and A_{tran} are the amplitude of the reflected wave, incident wave, and transmitted wave respectively. These calculations are based on the S-parameters described by Kurokawa in [36].

- Dispersion diagram: This curve describes how the phase of the wave varies between two points as a function of frequency. It is calculated from the S-parameters obtained in the FEM simulation, and then, the ABCD parameters are calculated analytically.

V. RESULTS

This section presents the results obtained from the detailed parametric study that allowed the identification of the final design. Subsequently, analytical and numerical studies were developed based on this design.

A. PARAMETRIC STUDY

A parametric study of various geometric characteristics of the antenna is conducted, including the unit cell length (thickness) t_{cell}, the shunt width w_{sh}, and the inner cell radius r_{in}. For this purpose, this study is carried out with the complete antenna and the frequency range is analyzed as a function of the radiation angle θ_r. The objective is to determine a geometry that allows the antenna to radiate in the widest possible bandwidth.

1) VARIATION OF THE THICKNESS OF THE UNIT CELL (T_{CELL})

Initially, the unit cell thickness is 16.5 mm and has been gradually increased to 56.5 mm in steps of 8 mm, as shown in Figure 7. The other parameters were kept constant, as indicated in Table 3. This figure shows an inverse relation between cell thickness and operating frequencies; it is clearly observed that as the thickness increases, the operating frequencies decrease. At the smallest thickness of 16.5 mm, the angular response remains more stable over a frequency range of 2700 Hz to 5400 Hz compared to the other thicknesses. This trend could be attributed to the acoustic properties of the cell geometry, which directly affects the antenna's resonance and, consequently, its operating frequency. On the other hand, although the increase in cell thickness is significant, the curves follow a clear trend, indicating that the changes in the angular response are gradual and predictable.

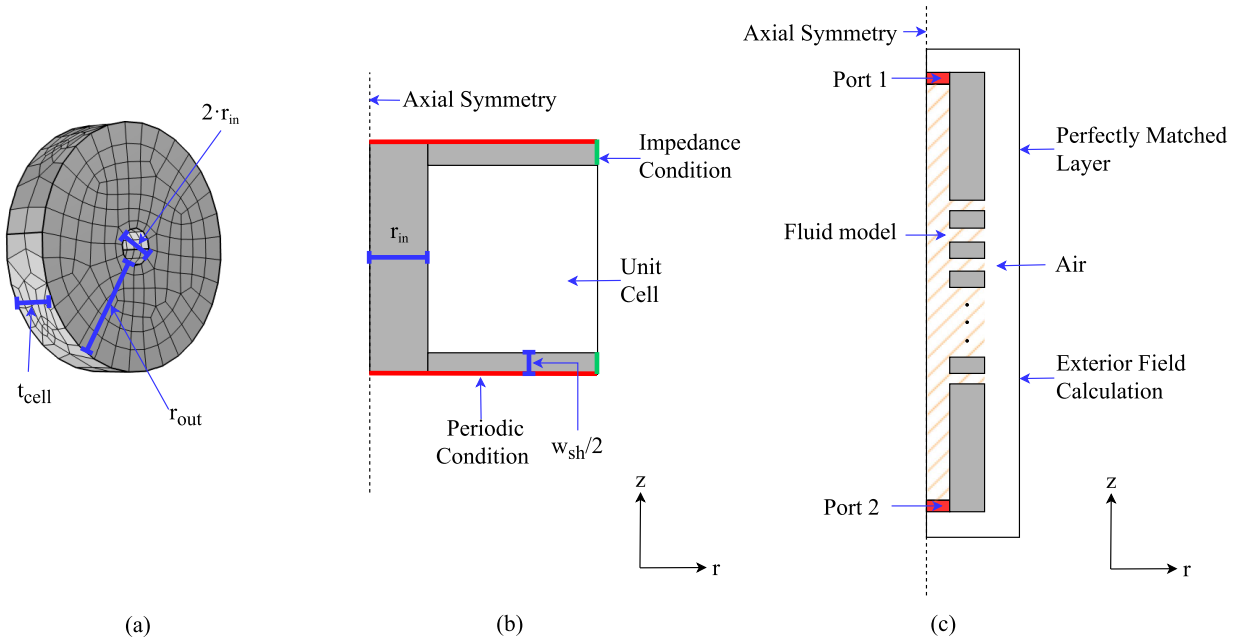

FIGURE 6. Boundary conditions of the ALWA in FEM simulation. (a) Example of mesh, (b) Unit cell, (c) Complete antenna structure.

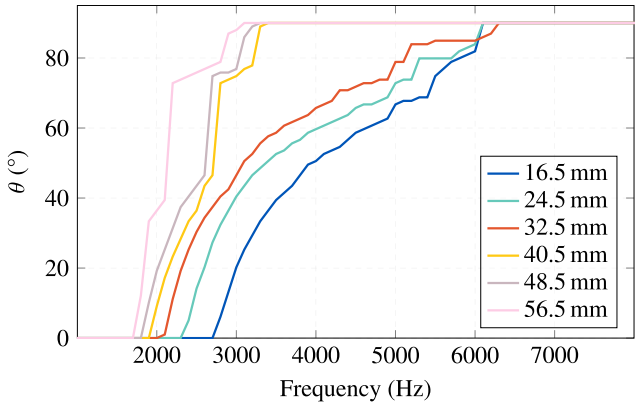

FIGURE 7. ALWA scanning angle for different thicknesses of the unit cell (t_{cell}).

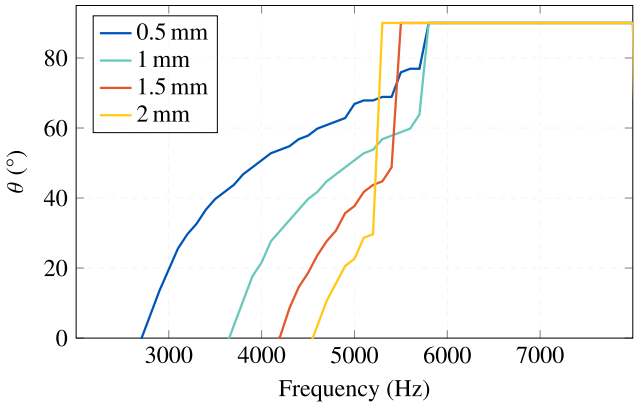

FIGURE 8. ALWA scanning angle for different shunt widths (w_{sh}).

2) VARIATION OF THE SHUNT WIDTH (W_{SH})

In this case, a parametric study is performed by varying w_{sh} from 0.5 mm to 2 mm in 0.5 mm increments. As in the previous case, the other parameters have been kept fixed according to the Table 3.

Fig. 8 shows that as w_{sh} increases, the working frequency range decreases and there is a shift toward higher frequencies. For example, for a w_{sh} of 2 mm, there is a frequency range between 4000 Hz and 5100 Hz, and for a width of 0.5 mm, there is a wider range between 2700 Hz to 5400 Hz.

3) VARIATION OF INNER CELL RADIUS (R_{IN})

The inner cell radius r_{in}, initially 3 mm, was varied up to 15 mm with steps of 3 mm, as shown in Fig. 9. With an r_{in} of 3 mm, an operating frequency range has been identified that extends from approximately 2700 Hz to 5800 Hz. This range is remarkably wide and allows a scanning angle reaching almost 90°, while for smaller radius it has smaller ranges, apart from dropping in frequency.

After carrying out a parametric study based on FEM simulations and comparing the different results obtained for t_{cell}, w_{sh} and r_{in} as a function of the working frequency range and the scanning angle, the values shown in Table 3 are obtained. The results selected for $t_{cell} = 16.5$ mm, $w_{sh} = 0.5$ mm and $r_{in} = 3$ mm indicate that the antenna can operate with a wider frequency bandwidth and a wider scan angle (blue curve in Fig.7, Fig.9 and Fig.8).

It is important to point out that the values presented correspond to the best results obtained within the set of

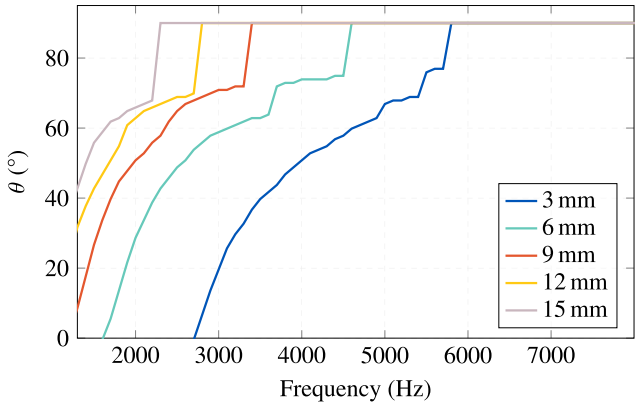

FIGURE 9. ALWA scanning angle for different inner cell radius (r_{in}).

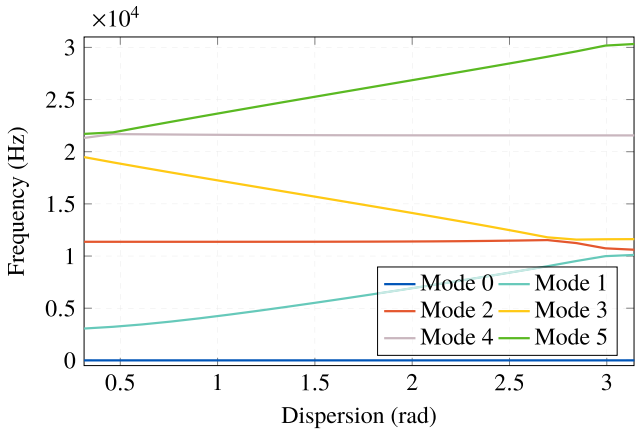

FIGURE 10. Banding structure. Represents the ALWA modes of operation of the first order.

configurations analyzed, although this does not guarantee that they are the maximum possible for this type of geometry at these frequencies.

TABLE 3. Geometric parameters of the proposed antenna.

Variable	Description	Value (mm)
l_{wg}	Input/output waveguide lengths	382
r_{in}	Inner cell radius	3
t_{cell}	Thickness of the unit cell	16.5
w_{sh}	Width of the shunt	0.5
r_{out}	Lenght of the wall	17

B. UNIT CELL

The unit cell simulation study focuses on band structure analysis to identify the working zones described in this research. The modes of a waveguide are solutions to the wave equation for a specific geometry. The obtained modes are shown in Fig. 10.

Calculating the cut-off frequency of the first higher order mode f_{mn}^c (1,1) [37] which is given by expression (22):

$$f_{mn}^c = \frac{\alpha'_{mn}\, c_0}{2\,\pi\, r_{in}} \tag{22}$$

where α'_{mn} corresponds to the nth zero of the derivative of the first-species Bessel function [29]. We obtain $f_{mn}^c = 30\,000$ Hz, which marks the limit from which higher order modes begin to propagate.

Working in the fundamental mode is preferable because it offers greater stability and control compared to higher modes, which tend to be more sensitive to system variations. In addition, the fundamental mode has lower attenuation, which allows for more efficient propagation with less energy loss. Its simpler and more symmetrical waveform facilitates system analysis and design, avoiding the complex interferences that usually arise in higher modes.

Initially, six modes are observed. However, the zero mode lacks physical significance and will not be considered. Thus, the analysis focuses on the remaining five modes. In the fundamental mode (cyan curve), a bandgap is identified at 10 kHz, corresponding to the Bragg frequency given by expression (23):

$$f_{Bragg} = \frac{c_0/2}{t_{cell}} \tag{23}$$

This frequency is observed when sound travels through the air and encounters a structure, such as a wall with evenly spaced holes. When acoustic waves at this frequency strike the structure, the scattering that results causes interference, which blocks wave propagation and creates a bandgap, as illustrated in Fig. 10.

The bandgap shown between the fundamental mode and the following mode is mainly due to the destructive interference induced by the periodicity of the structure and the scattering of waves at specific frequencies (f_{Bragg}). In an ALWA, this destructive interference is a product of the Bragg frequency in periodic structures, where the periodicity causes reflections at the interfaces that prevent wave propagation in certain frequency bands. Bandgap arises from a combination of phenomena such as acoustic wave scattering, changes in phase and group velocities, and mode coupling, which restrict the existence of stable solutions within those frequencies. Also, additional factors such as the geometry of the structure may influence the formation of this bandgap, in which acoustic waves cannot propagate efficiently.

C. 32 CELLS

This section presents the simulation results for the complete antenna, as shown in Fig. 6c. The relevant magnitudes described in Section IV are used for this analysis.

1) RADIATION PATTERN

The antenna radiation patterns are illustrated in Fig. 11. The directivity varies from 20° to 85° within the operating frequency range of 2700 Hz to 5441 Hz. At 2700 Hz, the radiation is oriented towards broadside, whereas at frequencies near the upper limit of the range, around 5000 Hz, the radiation shifts towards endfire. Furthermore, it is observed that as the frequency increases, the beam

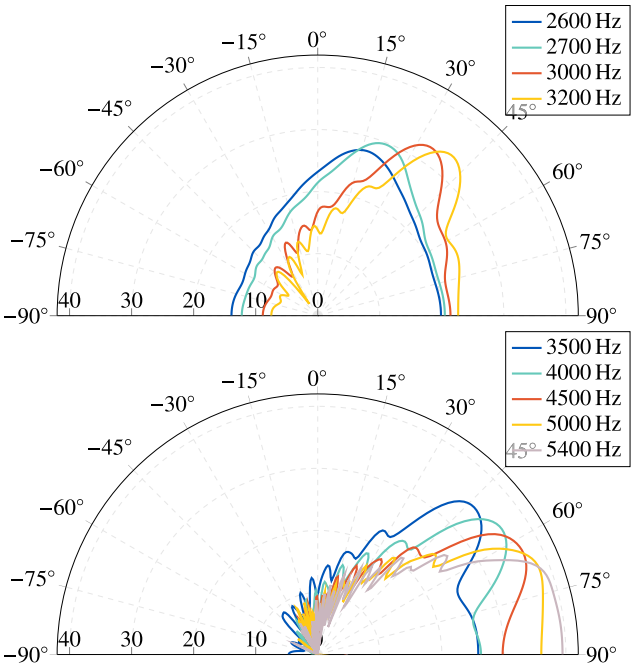

FIGURE 11. Radiation pattern of the ALWA.

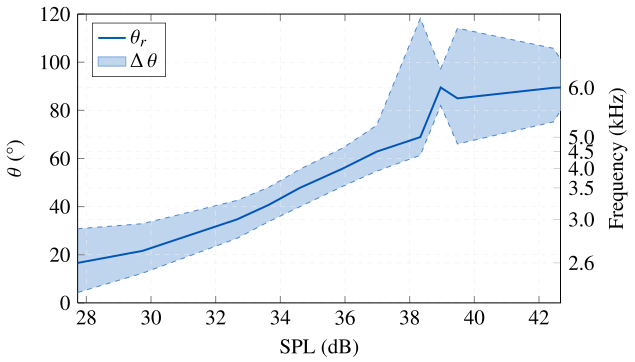

FIGURE 12. Numerical values of radiation pattern of the ALWA. Represents θ_r and $\Delta\theta$ as a function of frequency and SPL.

narrows and the SPL increases up to a frequency of 3500 Hz. This can be seen in Fig. 12 where presents the Sound Pressure Level (SPL), the beamwidth $\Delta\theta$ at -3 dB, and the radiation angle θ_r. In addition, it can be seen that θ_r and SPL increase as each excitation frequency increases. The maximum SPL is obtained at a frequency close to 6000 Hz.

At a frequency of $f_c = 4500$ Hz a scanning angle of 90° is obtained, as illustrated in the blue dashed curve in Fig.13 obtained theoretically. On the other hand, it is observed in the FEM simulation that to reach the endfire radiation is obtained at a frequency of about 5400 Hz, as seen in the color range (deep red). However, the beamwidth is wider, this may be due to interference generated by the antenna structure.

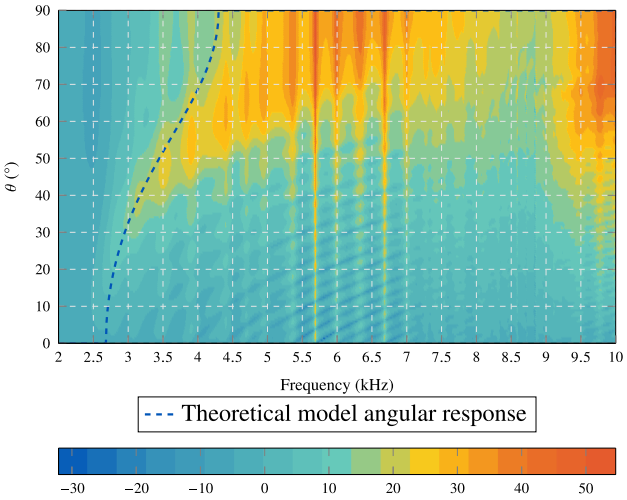

FIGURE 13. Comparison of the angular response of the theoretical model with the SPL (dB) of the numerical modeling of the ALWA. The dotted blue curve represents the theoretical model while the color range represents the numerical model.

In relation to the side lobes, Fig. 11 illustrates how they begin to appear as the frequency increases. This phenomenon is the result of constructive and destructive interference of the acoustic waves propagating through the periodic slots of the waveguide. As shown in Fig. 12, a progressive decrease in the HPBW is observed as the frequency increases, reaching a minimum around 4000 Hz. Beyond this point, the beamwidth begins to expand due to interference effects caused by interactions with the system structure. Finally, in Fig. 13, the SPL values corresponding to the main lobe are highlighted in red while the levels associated with the side lobes are shown in yellow.

These results demonstrate the antenna's capability to adjust its directivity based on frequency, achieving higher directivity as the frequency increases until reaches a frequency of 5000 Hz where the tendency is to become less directive. This continues until the theoretical cut-off frequency of 5441 Hz is approached.

2) REFLECTION AND TRANSMISSION PARAMETERS

Fig. 14 shows that within the working region, the transmission coefficient T is greater than the reflection coefficient R. This indicates that the incident wave is efficiently transmitted through the antenna, a desirable characteristic as it maximizes power transfer.

Ideally, in a lossless conservative system, the sum of the transmission and reflection coefficients should be equal to 1, reflecting the conservation of energy: $|R|+|T| = 1$. However, in practice, this condition is not perfectly fulfilled because of several intrinsic losses of the system, such as thermoviscous absorption and radiation losses. The latter is desirable in the system, since they allow the antenna to radiate power outside.

On the other hand, in Fig.14 we also have the radiation efficiency η_{rad}. It is observed that the radiation efficiency is

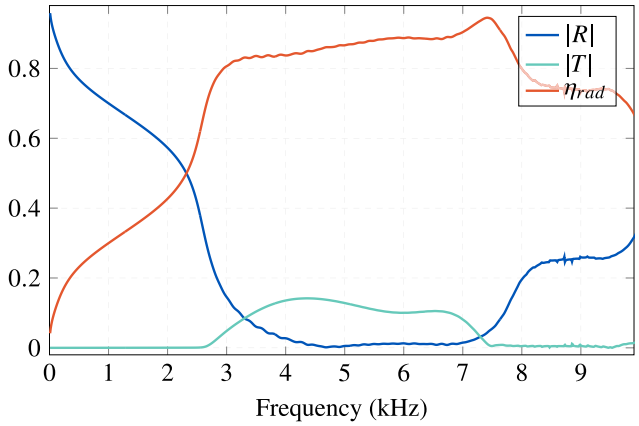

FIGURE 14. Transmission and reflection parameters of the ALWA.

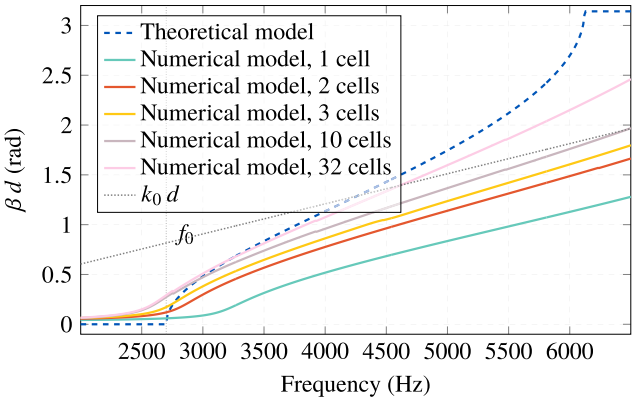

FIGURE 15. Theoretical and numerical ALWA dispersion diagram.

close to 1 in the frequency range where the antenna radiates power to the outside. This confirms that this is a conservative system.

As for the intrinsic losses, since the system operates in a frequency range where the radiation is almost total (close to 1), the thermoviscous losses have a negligible influence on the practical results. This simplification choice is consistent with the existing literature [11], [14].

As mentioned above, the narrow region acoustic boundary condition is used to model the propagation of sound waves in narrow ducts, where the thermal and viscous losses associated with the boundary layer are simplified. These losses, which result from the interaction between the fluid and the duct walls, are homogenized in the model to facilitate calculations. This approach is particularly effective for structures with small cross-sections relative to the acoustic wavelength, allowing efficient representation of wave attenuation and damping in simple geometries.

D. COMPARISON OF DIFFERENT CELL CONFIGURATIONS

This section presents the dispersion diagram of the ALWA with different cell configurations.

Fig. 15 illustrates the two regions: the fast wave zone and the slow wave zone, separated by the straight line $k_0\,d$. As the number of cells increases, the curves more closely resemble the analytical ones. This is because, with a greater number of leakages, the wave undergoes a phase shift due to interferences. In fact, single-cell analysis ignores these couplings, which have a crucial on the final performance. Therefore, it is necessary to model a cell in an environment where it is surrounded by identical cells. In the simulation, n-cells are used, from which the ABCD parameters are obtained. Subsequently, the n-th root is calculated to determine the value of β.

The choice of 32 cells in the antenna design is based on the need to achieve an appropriate balance between performance and total system length. As shown in Fig. 15, the analysis of the dispersion as a function of the number of cells shows that a higher number of cells improves the performance by getting closer to the theoretical model. However, an excessive increase in the number of cells also increases the overall antenna length, which could complicate its integration in practical applications. Therefore, opting for 32 cells represents a suitable compromise that maximizes performance without sacrificing the structural and operational feasibility of the design.

FIGURE 16. Unit cells built.

VI. MANUFACTURING AND EXPERIMENTAL MEASUREMENTS

This section describes the materials used in the fabrication of the ALWA antenna and presents the results of the measurements performed in the anechoic chamber with the prototype antenna.

The ALWA was constructed using methacrylate (PMMA) as the only material for the inlet and outlet waveguides as well as for the cells. This material was chosen for its excellent mechanical and acoustic properties.

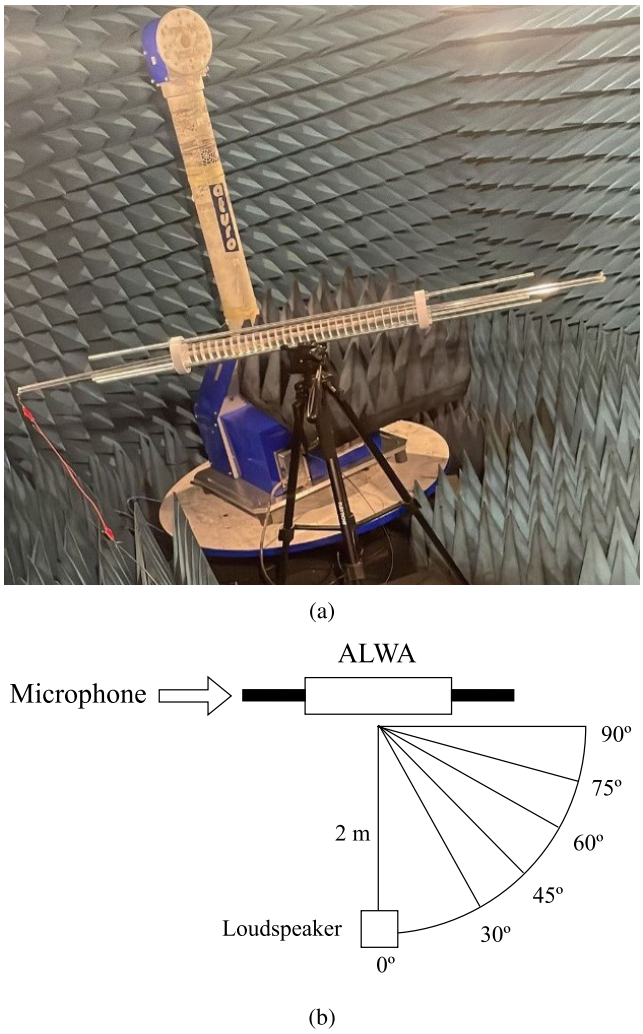

FIGURE 17. Experimental setup of the ALWA. (a) Photograph of the ALWA measurements in an anechoic chamber, (b) Schematic diagram of the experimental setup for directivity measurements.

From an acoustical point of view, methacrylate is classified as a rigid material, which is essential for applications where it is necessary to precisely control sound propagation. Acoustic stiffness refers to the ability of a material to resist deformation when exposed to acoustic pressure waves, which minimizes the loss of acoustic energy due to absorption or structural deformation. This property ensures that waveguides and cells maintain their structural integrity in the face of variations in acoustic pressure, thus guaranteeing efficient and predictable wave transmission.

The unit cells that have been constructed are shown in Fig. 16. In order to ensure a uniform spacing between them, steel wires have been used to maintain a controlled distance. In this case, the spacing achieved corresponds to the desired leakage, with a value of 0.5 mm.

Fig. 17a shows the antenna in its entirety, highlighting the two waveguides and the periodic region. The white end supports have a dual function: to secure the structure support and to ensure the exact alignment of the unit cells. These

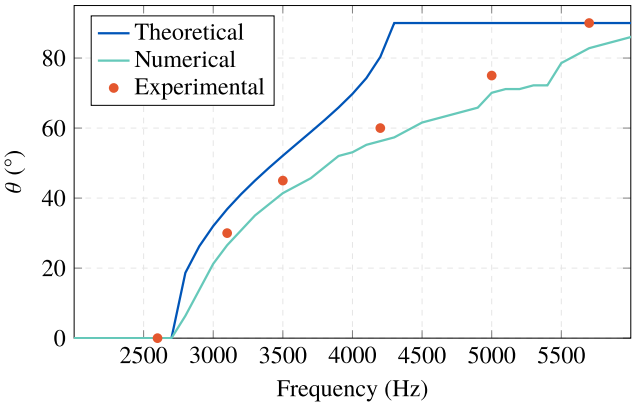

FIGURE 18. Theoretical, numerical and experimental comparison of the angular response of the ALWA.

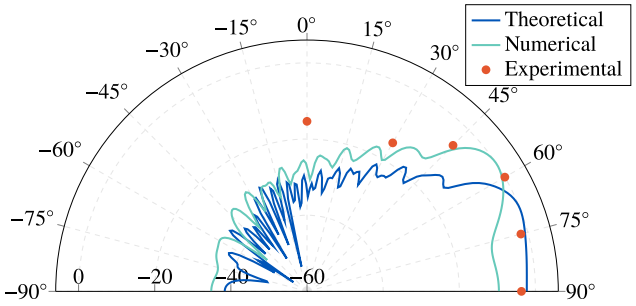

FIGURE 19. Radiation patterns of theoretical, numerical and experimental ALWA at a frequency of 4200 Hz.

brackets have been designed and manufactured using 3D printing, ensuring dimensional accuracy and adaptability to the required design.

On the other hand, measurements were performed using a microphone, model CMEJ-0627-42-P, which was placed at the end of the antenna. This configuration allowed the antenna to operate in receive mode to carry out the necessary measurements. With respect to the loudspeaker used, the NTi Audio TalkBox model was used.

The experiment consists of emitting white noise through a loudspeaker, moving it angularly from 0° to 90°, as shown in Fig. 17b. White noise is used because of its uniform content of all audible frequencies. According to the numerical simulation, the antenna operates in a frequency range from 2700 Hz to 7000 Hz. The loudspeaker was placed at distance of 2 m from the antenna.

The angular response of the ALWA is presented in Fig. 18, where the theorical, numerical and experimental results are compared. It can be observed that the numerical simulation agrees with the experimental measurements. However, a discrepancy with the analytical model is identified due to the fact that the FEM simulations take into account factors such as the coupling between cells and the acoustic loss model in narrow regions.

On the other hand, Fig. 19 shows a comparison of the radiation patterns of the three models analyzed: theoretical,

numerical and experimental. This example shows the radiation pattern of the experimental measurements compared to the theoretical and numerical models at a frequency of 4200 Hz. The results indicate a good agreement, which validates the theoretical and numerical models pointing to an angle close to 60°.

VII. CONCLUSION

In this work, a comprehensive analysis of the design of an ALWA has been carried out, covering different key stages. Initially, an acoustic concentrated element study was implemented, which laid the theoretical and functional foundations of the system. Subsequently, the TMM was applied to model the propagation of acoustic waves through periodic elements, which allowed characterizing the transmission and reflection properties of the antenna. In parallel, FEM simulations were used to simulate the system response to harmonic excitations, taking advantage of its ability to handle complex geometries and to establish the appropriate boundary conditions for the design of a symmetrical antenna. Finally, the final system design was fabricated and the results were validated by experimental measurements.

The parametric study with FEM simulation provided information on key geometrical parameters of the antenna, such as $t_{cell} = 16.5\,\text{mm}$, $w_{sh} = 0.5\,\text{mm}$ and $r_{in} = 3\,\text{mm}$, which were identified as the most suitable for its correct operation over a wide frequency range. These parameters, as in the case of LWAs, allow the directional behaviour of the antenna to be adjusted as a function of the operating frequency. In fact, as demonstrated in the FEM simulation, the variation of these values not only affects the operating frequency, but also the directionality of the radiation pattern. These have been chosen because the thickness of the cell, t_{cell}, affects both the propagation (expression 18) and the dispersion diagram (expression 19). On the other hand, both inner cell radius, r_{in}, and width of the shunt, w_{sh}, directly affect the shunt mass (expression 8) and indirectly the upper cutoff frequency, f_c, (expression 10). This analysis, together with the calculation of the radiation patterns, the scanning angle and the dispersion diagrams, allowed the theoretical behavior of the antenna to be validated. It was shown that the ALWA generates a highly directional radiation pattern, highlighting the importance of understanding the effect of cell number under different operating conditions.

The analysis of the band structure of the unit cell provided a detailed understanding of the modes and their operating frequencies, with special emphasis on the fundamental mode (mode 1) due to its wide frequency bandwidth, which enhances wave propagation through the structure and facilitates acoustic wave transmission over a wider range of frequencies.

The experimental measurements performed have effectively validated the results obtained from the numerical simulations, showing a good agreement between both. The experimental data confirmed the accuracy of the ALWA design, highlighting the effectiveness of the FEM simulations in predicting the acoustic behavior of the system. However, small discrepancies were noted that can be attributed to practical factors such as manufacturing tolerances and test conditions, which were not fully accounted for in the theoretical models. These experimental results reinforce the reliability of the approach used and provide a solid basis for future design improvements and optimizations.

This work demonstrates the disruptive potential of the ALWAs in the precise localization of sound sources and the possibility of significantly reducing the size and complexity of traditional acoustic devices, opening up new possibilities, particularly in underwater acoustic communications. Unlike hydrophone arrays, which consist of multiple hydrophones distributed in a specific configuration and tend to be bulkier and more complex, ALWA technology uses a single transducer and takes advantage of the phenomenon of diffraction of acoustic waves. This not only allows for more accurate and faster localization, but also reduces cost and facilitates deployment in complex environments where sound is affected by multiple factors, such as underwater acoustic communications.

REFERENCES

[1] C. Cheng, C. Wang, D. Yang, W. Liu, and F. Zhang, "Underwater localization and mapping based on multi-beam forward looking sonar," *Frontiers Neurorobotics*, vol. 15, Jan. 2022, Art. no. 801956.

[2] M. P. Hayes and P. T. Gough, "Synthetic aperture sonar: A review of current status," *IEEE J. Ocean. Eng.*, vol. 34, no. 3, pp. 207–224, Jul. 2009.

[3] M.-A. Chung, H.-C. Chou, and C.-W. Lin, "Sound localization based on acoustic source using multiple microphone array in an indoor environment," *Electronics*, vol. 11, no. 6, p. 890, Mar. 2022.

[4] L. Chen, G. Chen, L. Huang, Y.-S. Choy, and W. Sun, "Multiple sound source localization, separation, and reconstruction by microphone array: A DNN-based approach," *Appl. Sci.*, vol. 12, no. 7, p. 3428, Mar. 2022.

[5] D. R. Jackson, C. Caloz, and T. Itoh, "Leaky-wave antennas," in *Antenna Engineering Handbook*, vol. 100. Piscataway, NJ, USA: IEEE Press, 2012, pp. 2194–2206.

[6] C. J. Naify, C. N. Layman, T. P. Martin, M. Nicholas, D. C. Calvo, and G. J. Orris, "Experimental realization of a variable index transmission line metamaterial as an acoustic leaky-wave antenna," *Appl. Phys. Lett.*, vol. 102, no. 20, May 2013, Art. no. 203508.

[7] H. Esfahlani, S. Karkar, and H. Lissek, "Optimization of an acoustic leaky-wave antenna based on acoustic metamaterial," École Polytechn. Fédérale de Lausanne (EPFL), Lausanne, Switzerland, Tech. Rep., 2013.

[8] J. S. Rogers, C. J. Naify, M. Guild, C. A. Rohde, and G. J. Orris, "Evaluation of the resolution of a metamaterial acoustic leaky wave antenna," *J. Acoust. Soc. Amer.*, vol. 139, p. 2182, Apr. 2016.

[9] C. A. Rohde, M. D. Guild, and C. J. Naify, "Miniature acoustic leaky-wave antenna for ultrasonic imaging," U.S. Patent 15 246 798, Mar. 2, 2017.

[10] M. T. Akram, J.-Y. Jang, and K. Song, "Directional enhancement of triangular holographic acoustic leaky-wave antennas with reflectors," *Int. J. Mech. Sci.*, vol. 273, Jul. 2024, Art. no. 109216.

[11] F. Bongard, H. Lissek, and J. R. Mosig, "Acoustic transmission line metamaterial with negative/zero/positive refractive index," *Phys. Rev. B, Condens. Matter*, vol. 82, no. 9, Sep. 2010, Art. no. 094306.

[12] H. Esfahlani, S. Karkar, H. Lissek, and J. R. Mosig, "Exploiting the leaky-wave properties of transmission-line metamaterials for single-microphone direction finding," *J. Acoust. Soc. Amer.*, vol. 139, no. 6, pp. 3259–3266, Jun. 2016.

[13] Y. Xie, T.-H. Tsai, A. Konneker, B.-I. Popa, D. J. Brady, and S. A. Cummer, "Single-sensor multispeaker listening with acoustic metamaterials," *Proc. Nat. Acad. Sci. USA*, vol. 112, no. 34, pp. 10595–10598, Aug. 2015.

[14] C. W. Broadman, C. J. Naify, M. J. Lee, and M. R. Haberman, "Design of a one-dimensional underwater acoustic leaky wave antenna using an elastic metamaterial waveguide," *J. Appl. Phys.*, vol. 129, no. 19, May 2021, Art. no. 194902.
[15] Q. Wang, J. Lan, Z. Deng, Y. Lai, and X. Liu, "Acoustic source localization based on acoustic leaky-wave antenna with heterogeneous structure," *J. Acoust. Soc. Amer.*, vol. 153, no. 1, pp. 487–495, Jan. 2023.
[16] I. Felis-Enguix, J. Otero-Vega, M. Campo-Valera, I. Villó-Pérez, and J. Gómez-Tornero, "Practical aspects of acoustic leaky-wave antennas applied to underwater direction finding," *Eng. Proc.*, vol. 2, no. 1, p. 93, 2020.
[17] C. J. Naify, C. A. Rohde, T. P. Martin, M. Nicholas, M. D. Guild, and G. J. Orris, "Generation of topologically diverse acoustic vortex beams using a compact metamaterial aperture," *Appl. Phys. Lett.*, vol. 108, no. 22, May 2016, Art. no. 223503.
[18] F. Monticone and A. Alú, "Leaky-wave theory, techniques, and applications: From microwaves to visible frequencies," *Proc. IEEE*, vol. 103, no. 5, pp. 793–821, May 2015.
[19] M. Lee, C. Wiederhold, K. Spratt, C. J. Naify, and M. R. Haberman, "Experimental demonstration of an underwater acoustic leaky wave antenna," *J. Acoust. Soc. Amer.*, vol. 145, p. 1727, Mar. 2019.
[20] J. Zhang, V. Romero-García, G. Theocharis, O. Richoux, V. Achilleos, and D. J. Frantzeskakis, "High-amplitude sound propagation in acoustic transmission-line metamaterial," *Appl. Phys. Lett.*, vol. 118, no. 10, Mar. 2021, Art. no. 104102.
[21] C. J. Naify, M. D. Guild, C. A. Rohde, D. C. Calvo, and G. J. Orris, "Demonstration of a directional sonic prism in two dimensions using an air-acoustic leaky wave antenna," *Appl. Phys. Lett.*, vol. 107, no. 13, Sep. 2015, Art. no. 133505.
[22] Z. Zhu, Y. Zhou, R. Wang, and F. Tong, "Internet of underwater things infrastructure: A shared underwater acoustic communication layer scheme for real-world underwater acoustic experiments," *IEEE Trans. Aerosp. Electron. Syst.*, vol. 59, no. 5, pp. 6991–7003, Oct. 2023.
[23] F. Bongard, H. Lissek, and J. R. Mosig, "Transmission line based metamaterials for acoustic waves," in *Proc. 30th URSI Gen. Assem. Sci. Symp.*, Aug. 2011, pp. 1–4.
[24] C. Caloz and T. Itoh, *Electromagnetic Metamaterials: Transmission Line Theory and Microwave Applications*. Hoboken, NJ, USA: Wiley, 2005.
[25] L. E. Kinsler, A. R. Frey, A. B. Coppens, and J. V. Sanders, *Fundamentals of Acoustics*. Hoboken, NJ, USA: Wiley, 2000.
[26] S. Lim, C. Caloz, and T. Itoh, "Metamaterial-based electronically controlled transmission-line structure as a novel leaky-wave antenna with tunable radiation angle and beamwidth," *IEEE Trans. Microw. Theory Techn.*, vol. 52, no. 12, pp. 2678–2690, Dec. 2004.
[27] F. J. Villegas, D. R. Jackson, J. T. Williams, and A. A. Oliner, "Leakage fields from planar semi-infinite transmission lines," *IEEE Trans. Microw. Theory Techn.*, vol. 47, no. 4, pp. 443–454, Apr. 1999.
[28] D. R. Jackson, C. Caloz, and T. Itoh, "Leaky-wave antennas," *Proc. IEEE*, vol. 100, no. 7, pp. 2194–2206, Jul. 2012.
[29] D. T. Blackstock, *Fundamentals of Physical Acoustics*. Hoboken, NJ, USA: Wiley, 2000.
[30] H. Lissek, H. Esfahlani, S. Karkar, and J. R. Mosig, "Développement et validation d'une d'antenne acoustique á ondes de fuite," École Polytechn. Fédérale de Lausanne (EPFL), Lausanne, Switzerland, Tech. Rep., 2016.
[31] C. J. Naify, J. S. Rogers, M. D. Guild, C. A. Rohde, and G. J. Orris, "Evaluation of the resolution of a metamaterial acoustic leaky wave antenna," *The J. Acoust. Soc. Amer.*, vol. 139, no. 6, pp. 3251–3258, 2016.
[32] D. M. Pozar, *Microwave Engineering: Theory and Techniques*. Hoboken, NJ, USA: Wiley, 2021.
[33] T. J. Hughes, *The Finite Element Method: Linear Static and Dynamic Finite Element Analysis*. North Chelmsford, MA, USA: Courier Corporation, 2012.
[34] *COMSOL Multiphysics*, CAE-Service LLC, Moscow, Russia, 2014.
[35] R. W. Pryor, *Multiphysics Modeling Using COMSOL 5 and MATLAB*. Dulles, VA, USA: Mercury Learning and Information, 2021.
[36] K. Kurokawa, "Power waves and the scattering matrix," *IEEE Trans. Microw. Theory Techn.*, vol. MTT-13, no. 2, pp. 194–202, Mar. 1965.
[37] J. Price, "*Acoustic Waveguides*. Boulder, CO, USA: University of Colorado, vol. 22, 2008.

ALEJANDRO FERNÁNDEZ-GARRIDO was born in Linares, Jaén, Spain, in 1995. He received the degree in telecommunication technology engineering with double mention in sound and image and telecommunication systems from Universidad de Jaén (UJA), Spain, in 2020, and the master's degree in telecommunication engineering and the Ph.D. degree in information and communication technologies from Universidad Politécnica de Cartagena (UCPT), in 2023. His Ph.D. is about underwater acoustic communications designing acoustic leaky-waves antennas.

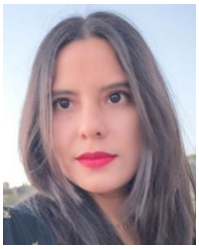

MARÍA CAMPO-VALERA was born in Santa Marta, Colombia, in 1984. She received the B.Sc. degree in sound engineering from San Buenaventura University, Bogotá, Colombia, in 2009, the M.Sc. degree in acoustic engineering from Universitat Politécnica de València (UPV), Spain, in 2016, and the Ph.D. degree from Universidad Politécnica de Cartagena (UPCT), Spain, in 2020. In January 2021, she was a Postdoctoral Researcher with UPCT. In January 2022, she joined Universidad de Málaga, Spain, as a Postdoctoral Researcher awarded a competitive two-year grant, named Margarita Salas (fully funded by the European Commission). She was a Visiting Researcher with the Escuela Naval de Cadetes Almirante Padilla (ENAP), Cartagena, Colombia. Currently, she is a Lecturer with Universidad de Málaga. Her research interests include signal processing, sensor design, nonlinear acoustics, and underwater acoustic communications.

ELENA ABDO-SÁNCHEZ (Member, IEEE) received the M.Sc. and Ph.D. degrees in telecommunication engineering from Universidad de Málaga, Málaga, Spain, in 2010 and 2015, respectively.

In 2009, she was a Granted Student with German Aerospace Center (DLR), Institute of Communications and Navigation, Munich, Germany. In 2010, she joined the Department of Communication Engineering, Universidad de Málaga, where became an Associate Professor, in 2021. From April 2013 to July 2013, she was a Visiting Ph.D. Student with the Antennas and Applied Electromagnetics Laboratory, University of Birmingham, Birmingham, U.K. From May 2016 to May 2017, she was a Marie Skłodowska-Curie Postdoctoral Fellow with the Electromagnetics Group, University of Toronto, Toronto, ON, Canada. Her research interests include electromagnetic analysis and design of planar antennas and the application of metasurfaces to the implementation of novel antennas.

Dr. Abdo-Sánchez was a recipient of the Junta de Andalucía Scholarship, from 2012 to 2015, the Marie Skłodowska-Curie Fellowship, from 2016 to 2018, and the Juan de la Cierva Fellowship, from 2020 to 2021.

RUBÉN PICÓ received the degree in physics from Universitat de València (UV), Spain, in 1999. He obtained his European Doctorate from the Universitat Politècnica de València (UPV), Spain, in 2004, and the title of Docteur en Acoustique from the University of Le Mans, France. Currently, he is a Full Professor with the Department of Applied Physics, UPV. He has participated in 48 research projects, of which he has led 13 as the Principal Investigator. This includes three technology transfer projects with the European Space Agency. He has worked across various fields of acoustics, including sonic crystals, acoustic metamaterials, periodic media, sound absorption in textiles, and ultrasound. He is (co-)author of over 60 scientific publications, 50 of which are articles published in high-impact journals, and he has contributed to more than 100 national and international conferences. He has supervised seven doctoral theses and is supervising three more. He serves as a reviewer for ten ISI-JCR journals in the field of acoustics.

ANTONIO-JAVIER GARCIA-SANCHEZ received the M.S. degree in industrial engineering from Universidad Politècnica de Cartagena (UPCT), Spain, in 2000, and the Ph.D. degree from the Department of Information Technologies and Communications (DTIC), UPCT, in 2005. He has been a Visiting Scholar with Bologna University, Italy, since 2007, Wageningen University, The Netherlands, since 2012, and Santiago de Cali University, Colombia, since 2019. Currently, he is a Full Professor with UPCT and the Head of DTIC. He is the (co-)author of more than 100 conference and journal papers, fifty-two of them indexed in *Journal Citation Report* (JCR). He has been the Head of several research projects in the field of communication networks and optimization. He is the inventor/co-inventor of 12 patents or utility models. He has been a TPC member or the Chair of about forty international congresses or workshops. He is a reviewer of several journals listed in the ISI-JCR. His main research interests include wireless sensor networks (WSNs), streaming services, artificial intelligence, the IoT, and nanonetworks.

RAFAEL ASOREY-CACHEDA (Member, IEEE) received the M.Sc. degree in telecommunication engineering (major in telematics) and the Ph.D. degree (cum laude) in telecommunication engineering from Universidade de Vigo, Spain, in 2006 and 2009, respectively. He was a Visiting Scholar with New Mexico State University, USA, from 2007 to 2011, and Universidad Politécnica de Cartagena, in 2011 and 2015. From 2008 and 2009, he was a Research and Development Manager with Optare Solutions, a Spanish telecommunications company. He was a Researcher with the Information Technologies Group, University of Vigo, Spain, until 2009. From 2009 to 2012, he held an Ángeles Alvari no position with Xunta de Galicia, Spain. From 2012 to 2018, he was an Associate Professor with the Centro Universitario de la Defensa en la Escuela Naval Militar, Universidade de Vigo. Currently, he is an Associate Professor with Universidad Politécnica de Cartagena, Spain. He is the author or the co-author of more than 70 journal and conference papers, mainly in the fields of switching, wireless networking, and content distribution. His research interests include content distribution, high-performance switching, peer-to-peer networking, wireless networks, and nano-networks. He received the Best Master Thesis Award for the M.Sc. degree and the Best Ph.D. Thesis Award for the Ph.D. degree.